Microfluid Nanofluid (2014) 17:1105–1112
DOI 10.1007/s10404-014-1399-6

RESEARCH PAPER

Fluid behavior of supercritical carbon dioxide with water in a double-Y-channel microfluidic chip

S. Ogden · R. Bodén · M. Do-Quang · Z. G. Wu · G. Amberg · K. Hjort

Received: 5 November 2013 / Accepted: 7 April 2014 / Published online: 23 April 2014

Abstract The use of supercritical carbon dioxide ($scCO_2$) as an apolar solvent has been known for decades. It offers a greener approach than, e.g., hexane or chloroform, when such solvents are needed. The use of $scCO_2$ in microsystems, however, has only recently started to attract attention. In microfluidics, the flow characteristics need to be known to be able to successfully design such components and systems. As supercritical fluids exhibit the exciting combination of low viscosity, high density, and high diffusion rates, the fluidic behavior is not directly transferrable from aqueous systems. In this paper, three flow regimes in the $scCO_2$–liquid water two-phase microfluidic system have been mapped. The effect of both total flow rate and relative flow rate on the flow regime is evaluated. Furthermore, the droplet dynamics at the bifurcating exit channel are analyzed at different flow rates. Due to the low viscosity of $scCO_2$, segmented flows were observed even at fairly high flow rates. Furthermore, the carbon dioxide droplet behavior exhibited a clear dependence on both flow rate and droplet length.

Keywords Two-phase flow · Segmented flow · Parallel flow · Wavy flow · Droplet dynamics

1 Introduction

Supercritical carbon dioxide ($scCO_2$) can, due to its liquid-like density, gas-like viscosity, and diffusion rate in-between that of a gas and a liquid, be used as an environmentally friendly solvent, replacing solvents, such as hexane or chloroform, in the extraction of apolar compounds. Recently, this has attracted the attention of the microfluidic community, resulting in supercritical microfluidic applications, such as particle synthesis, microreactors, and flow-through chemistry, as presented in a recent review (Marre et al. 2012). In addition to the applications presented in that review, $scCO_2$ is used in analytical chemistry, such as supercritical fluid chromatography, SFC (Lee and Markides 1990), and in extraction and synthesis in green technologies (Herrero et al. 2010). There are good reasons to pursue miniaturization also for these applications. Depending on the focus of interest, the laminar flow should be parallel, segmented, or having droplets in a surrounding matrix. Also, for many of these applications using two-phase flow, it is interesting to control the exit behavior of the two phases, e.g., when one of them contains the substances of interest while the other one is waste. Hence, to allow for design of $scCO_2$ microfluidics, there is a need of a better understanding of the fluid behavior at smaller scale.

Droplet microfluidics has been used, especially in chemistry, to create well-defined minute and discrete volumes in which a batch reaction or efficient molecular transfer between droplets and matrix can take place (Squires and Quake 2005). The dynamics of microfluidic droplets have been extensively studied in a multitude of different geometric configurations (Baroud et al. 2010; Nightingale and DeMello 2013). Recently, the droplet dynamics, especially the splitting behavior, at a bifurcating channel were modeled (Carlson et al. 2010).

Previously, the use of $scCO_2$ for extraction has been shown in a microfluidic Y-channel (Ohashi et al. 2011), as well as in a T-shaped inlet (Assmann et al. 2012). In the

S. Ogden · R. Bodén · Z. G. Wu · K. Hjort (✉)
Micro Systems Technology,
Uppsala University, Uppsala, Sweden
e-mail: klas.hjort@angstrom.uu.se

M. Do-Quang · G. Amberg
Fluid Mechanics, Royal Institute of Technology,
Stockholm, Sweden

work of Ohashi et al. (2011), a parallel flow profile was utilized to determine the distribution behavior of tris(acetylacetonato)cobalt(III) from the $scCO_2$ phase to the water phase. In the work of Assmann et al. (2012), a segmented flow was used to extract vanillin from the water phase to the $scCO_2$ phase. Although microfluidic devices, these studies focused on the extraction capabilities of the system, with only one set of flow parameters presented.

The microfluidics of two-phase flows where $scCO_2$ is one of the phases has been previously studied in a T-junction with ethanol and methanol (Blanch-Ojea et al. 2012), and in annular flow with water (Marre et al. 2009; Guillaument et al. 2013). In the work of Blanch-Ojea et al. (2012), the authors studied the effect of varying pressure and temperature in these $scCO_2$–ethanol and $scCO_2$–methanol systems, using a glass microfluidic chip. In the works of Marre et al. (2009) and Guillaument et al. (2013), coaxially mounted silica capillaries were used to map the dripping to jetting transition regions of a $scCO_2$–water system, as well as to model the influence of wall surface tension and interfacial tension between the fluids. Although both these cases are closely related to this work, the use of ethanol and methanol differs from the use of water, as they are miscible with $scCO_2$. Furthermore, the fluid dynamics differ somewhat between annular co-flow and two flows joining at a Y-intersection.

In this study, the transition from segmented to parallel flow in a microfluidic Y-channel is mapped for the first time. The mapping is done with respect to both total flow rate and the relative flow rates of the two phases. Furthermore, the exit behavior of both water and $scCO_2$ droplets at the bifurcating exit is studied.

2 Theoretical background

In microfluidics, the use of dimensionless numbers to easier classify and understand the flow behavior is common. The three dimensionless numbers that are applicable to this work are the Reynolds number, *Re*, the capillary number, *Ca*, and the Weber number, *We*.

The Reynolds number is defined according to Eq. 1,

$$Re = \frac{\rho v L}{\eta} \tag{1}$$

where ρ is the fluid density, v is the fluid velocity, L is the characteristic length of the system, and η is the dynamic viscosity of the fluid. By balancing the inertial forces with the viscous forces, *Re* can be used to predict if a flow is laminar or turbulent, with the latter being uncommon in microfluidic flows due to the small characteristic lengths.

The capillary number balances the viscous forces with the interfacial tension and is defined according to Eq. 2,

$$Ca = \frac{\eta v}{\gamma} \tag{2}$$

where γ is the interfacial tension between the two fluids. This number can function as a guideline to whether the flow will be parallel, with the fluids flowing alongside each other, or break up into droplets and plugs.

If the viscosities in the fluids are kept constant, as in this study, the Weber number can be used, combining the Reynolds and capillary numbers according to Eq. 3,

$$We = Re \cdot Ca = \frac{\rho v^2 L}{\gamma} \tag{3}$$

thus representing the ratio between inertial and interfacial forces.

In the $scCO_2$/water system, some interdiffusion between fluids occurs, especially dissolution of CO_2 in water of a few percent (Liu et al. 2012).

The transition from stratified parallel flow to segmented flow has been the subject of several previous studies in a variety of channel dimensions (Ribatski 2013). Although stratified flow is not explicitly studied in this paper, the most interesting of these is the work of Barnea et al. (1983), where they argued that in small-diameter channels, the dominance of surface tension rather than the Kelvin–Helmholtz instability dictates the transition between these flows according to Eq. 4.

$$D - h_L \leq \frac{\pi}{4}\left[\frac{\sigma}{\rho g\left(1-\frac{\pi}{4}\right)}\right]^{1/2} \tag{4}$$

where D is the channel diameter, h_L is the water depth, σ is the surface tension, ρ is the liquid density, and g is the gravitational constant. This equation is always satisfied when D is smaller than the right-hand side of Eq. 4, which is the case for our experiments. For this case, Barnea et al. (1983) suggested a simplified transition criterion based on mass balance, Eq. 5.

$$h_L \geq \left(1-\frac{\pi}{4}\right)D \tag{5}$$

3 Experimental

The microfluidic chip, custom-made by Dolomite Ltd. (UK), consists of two 2-mm-thick borosilicate glass wafers bonded together and has a Y-intersection at both the inlet and outlet, Fig. 1. All channels have elliptic cross sections with half-axes measuring 90 and 87.5 μm, respectively. The chip is interfaced by gluing (araldite rapid) fused silica capillaries (Upchurch Scientific, 75 μm inner and 150 μm outer diameter) to the inlets and outlets. The two outlet capillaries are connected to a T-junction with an additional fused silica capillary as the single outlet. This capillary has an inner diameter of either 25 or

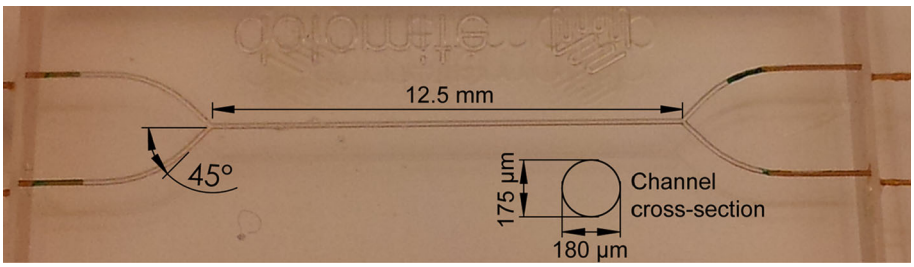

Fig. 1 Photograph of the microfluidic glass chip

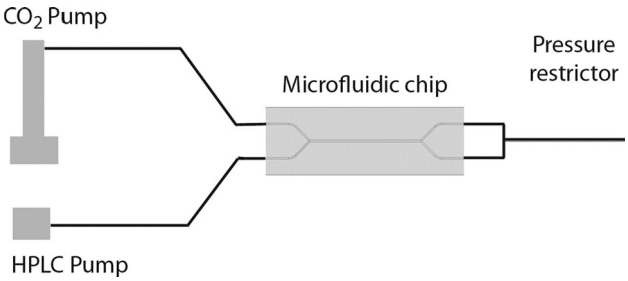

Fig. 2 Schematic view of the experimental setup

75 µm, depending on the flow rate setting, and is functioning as a pressure restrictor.

Food-grade CO_2 (99.5 % purity) was fed to the chip in liquid state using a high-pressure syringe pump (100 DM, Teledyne ISCO, USA), and green-dyed deionized water was supplied using a reciprocating dual piston HPLC pump (PU 980, JASCO International Co. Ltd., Japan). The chip is placed on a hotplate controlling the temperature. A schematic chart of the fluidic setup is shown in Fig. 2. Flow characteristics were evaluated using a high-speed camera (Phantom Miro M310, Vision Research Inc., USA), operating at 1,000 fps, connected to a microscope. In all experiments, the pressure was set to 10 MPa and the temperature to 50 °C. Three different total flow rates were evaluated, 20, 80, and 160 µL/min, with different lengths and diameters of the pressure restricting capillary used to maintain the same pressure regardless of total flow rate. The length of the capillary needed was calculated using Eq. 6,

$$Q = \pi \frac{\Delta p r^4}{8 \eta l} \tag{6}$$

where Q is the flow rate, Δp is the pressure difference over the capillary, r is the radius, η is the dynamic viscosity, and l is the length of the capillary. For the lowest flow rate, 20 µL/min, the capillary with 25 µm inner diameter was used, whereas capillaries with 75 µm inner diameter were used for the higher flow rates (80 and 160 µL/min). The use of different-diameter capillary restrictors is due to the short lengths required for the higher flow rates when using a 25 µm inner diameter capillary, 7.5 and 3.75 cm, respectively. If such short capillaries are used, the expansion and subsequent cooling of the CO_2 become too rapid, with a resulting ice clogging of the capillary.

For this behavior, the viscosity of water was used to calculate the lengths needed. For a high relative flow of water, this approximation is sufficient. For higher relative flows of CO_2, the flow resistance is smaller due to the lower viscosity of the two-phase fluid. To maintain the flow resistance in these cases, the capillary should be prefilled with water.

Table 1 shows the dimensionless numbers for the flow conditions used. The numbers are calculated with an interfacial surface tension of the H_2O–CO_2 system of 30 mN/m from Georgiadis et al. (2010). Furthermore, the densities of CO_2 and H_2O are 384 and 963 kg/m^3, respectively, and the viscosities are 32.6×10^{-6} and 5.5×10^{-4} Pa s, respectively (Linstrom and Mallard 2014).

Within the same total flow rate, the relative flow rate, $Q_{rel} = Q_{CO_2}/Q_{H_2O}$, was varied within the range: $1/9 \leq Q_{rel} \leq 9$.

The droplet lengths were measured directly from the high-speed movies using the channel width as reference.

Although the temperature is only controlled at the bottom surface of the chip, the higher thermal mass of the chip as well as the short diffusion lengths within the chip will ensure that thermal equilibrium will be reached before the Y-intersection.

Most of the pressure drop occurs in the restricting capillary on the chip's outlets; hence, the pressure drop along the channel is insignificant.

The velocities are estimated using volumetric flow rate and the steady-state temperatures, meaning that velocity variations are likely to occur at the inlet during heating. However, at the junction, steady state is already obtained, and thus, no further change in velocity should be due to density variations.

The density variations in the $scCO_2$ are expected to be small, in view of the expected pressure variations in the flow. If they would, however, make themselves felt, it would be seen as a slight compressibility or "elasticity" of the droplets that would allow them to change their volume as they would pass from high- to low-pressure regions. Gravity effects are not expected due to the small size of the systems.

Table 1 Dimensionless numbers for the different flow conditions used in the experiments

Total flow rate (μL/min)	Flow velocity (mm/s)	Dimensionless numbers					
		CO_2			Water		
		Re	*Ca*	*We*	*Re*	*Ca*	*We*
20	10.6	46	1.2×10^{-5}	5.5×10^{-4}	3.7	1.9×10^{-4}	7.0×10^{-4}
80	42.4	182	4.6×10^{-5}	8.4×10^{-3}	14.8	7.7×10^{-4}	0.01
160	84.8	364	9.2×10^{-5}	0.03	29.7	1.5×10^{-3}	0.04

4 Results and discussion

4.1 Flow regimes

Three different flow regimes have been identified within the set of flow parameters studied: parallel, wavy, and segmented, Fig. 3. However, due to flow rate variations in the HPLC pump, the presence of parallel and wavy flow was appearing, disappearing, and reappearing in a cyclic manner. When a flow is classified as a parallel or wavy flow in this work, it means that it at some point, in a stable manner, exhibits this type of flow.

Whereas the segmented flow is obviously different from the two other regimes, the difference between parallel and wavy flow is not as pronounced. The first difference between parallel and wavy flow is the shape of the interface, straight or wavy, and the other definition used here is that a parallel flow stays that way throughout the channel length, whereas the wavy flow eventually breaks up into segmented flow.

Figure 4 charts the flow regimes observed at the junction of the two inlet channels. From the figure, it is obvious that an increased total flow rate shifts the flow regime from segmented to parallel flow. It can also be seen that a low Q_{rel} (below 0.6) at a high total flow rate is destabilizing, as the parallel flow turns into wavy flow. Furthermore, a high Q_{rel} seems beneficial to achieve parallel flow as this was observed at 80 μL/min with a Q_{rel} exceeding 1.67. A possible explanation for these trends can be found in the fact that the glass has a hydrophilic surface. At lower flow rates, and consequently lower capillary numbers, the water is allowed to minimize its surface energy by adhering to the channel walls, effectively creating plugs. At higher flow rates, this possibility to equilibrate is removed. This phenomenon was also observed and characterized for a T-junction by Guillot and Colin (2005), where an increase

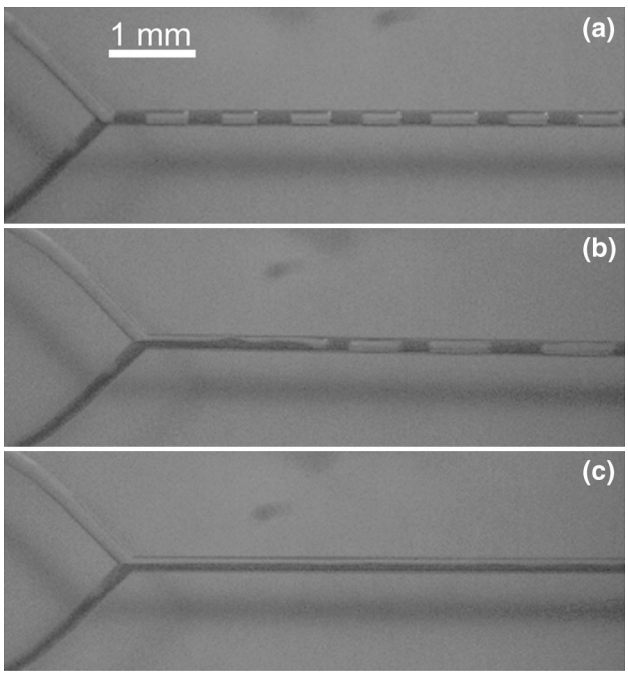

Fig. 3 Three different flow regimes observed: **a** segmented, **b** wavy, and **c** parallel. In the images, $scCO_2$ is transparent and water is opaque

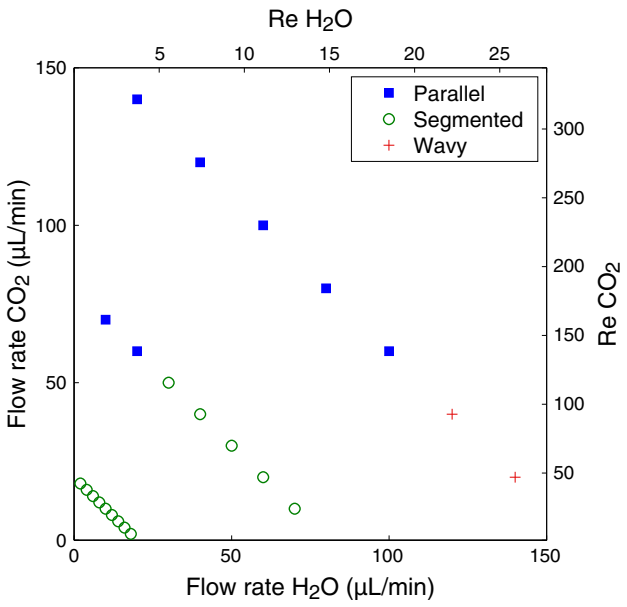

Fig. 4 Measured flow regime map with respect to flow rates and Reynolds numbers. Each measurement series (*diagonally*) correspond to a *Re*, *Ca*, and *We* number found in Table 1

in dispersed phase velocity induced parallel flow at a lower critical Ca.

Two-phase flows in tubes have been studied extensively in the literature, even though generally for larger flow rates and pipe dimensions, and not for supercritical fluids. However, there are some studies that are comparable in size, and if we compare our flow regime map in Fig. 4 with for instance Fig 6(a) in Yue et al. (2008), we see that our parameter range is at relatively small Reynolds numbers and falls entirely inside their slug flow regime. We notice that the differences are due to different relative importance of surface tension and wetting properties, as well as the fact that the density and viscosity ratios for $scCO_2$ and water are not in the range of conventional two-phase flows.

This corresponds well to the results in this study as a higher Q_{rel} corresponds to higher dispersed phase flow. Wetting characteristics can also be used to explain the fact that high Q_{rel}-flows form parallel flows easier than low Q_{rel}-flows. At higher Q_{rel}, there would only be enough water to form very narrow plugs, which would not reduce the total surface energy. The observations of wavy flow at a low Q_{rel} as well as parallel flow at lower flow rates at a high Q_{rel} also correspond to the transition criterion formulated by Barnea et al. (1983), shown in Eq. 5, where a decreased water depth in the channel favors parallel flow over segmented. Although this criterion cannot be used as the sole explanation of the transitions observed, as the total flow rate is not accounted for, it does predict that a high Q_{rel} favors parallel flow. According to the equation, the transition from parallel to segmented flow would occur at a liquid film thickness of 43 μm or higher. This value does not correspond well to the observations made here. However, as the criterion was based on observations in flow channels with a diameter between 4 and 12 mm, it is likely that a reduction in diameter with a factor 20–60 would affect the constants in Eq. 5 as it further increases the dominance of surface tension.

The reason the wavy regime is not observed at the lower flow rates is likely that a sufficiently high velocity, and consequently sufficiently high Reynolds number, is required. This map also corresponds with the modeling work previously done by Tammisola et al. (2011), where the effect of surface tension on the stability of a two-phase flow was evaluated. The study concluded that a high surface tension, and thus a low *We* stabilizes the flow, within the range evaluated, $2 < We < \infty$. If the *We* number is decreased even further, the surface tension would dominate the flow type completely, resulting in the segmented flow found at lower *We*.

Although some dissolution of CO_2 in water occurs, the dynamics also have to be accounted for. With the geometry investigated here, at least 12 s would be required for the system to equilibrate. As the lowest flow rate evaluated would pass through the main channel in approximately 1 s, the system will not be at equilibrium.

4.2 Droplet behavior at bifurcating exit

The exit behavior of droplets varies significantly between the two fluids. Since water wets the surface, water plugs always, independently of flow parameters, split at the exit. As seen in Fig. 5, the plug wets the walls on both exit channels. As it is equally drawn into both channels, the droplet eventually splits.

The behavior of $scCO_2$ droplets, however, is not independent of flow parameters. Both Ca, which is directly coupled to the flow rate, and the droplet volume affect the droplet behavior. With an increasing volume, and hence an increasing droplet length, the droplet will be more prone to splitting. The flow rate influence is similar; an increase in flow rate increases the possibility to split the droplet at the bifurcation. The maximum non-splitting droplet length observed was 2,080, 1,160, and 350 μm at 20, 80, and 160 μL/min flow rates, respectively. These results correspond well with the modeled results from Carlson et al. (2010), where a splitting–non-splitting regime map was

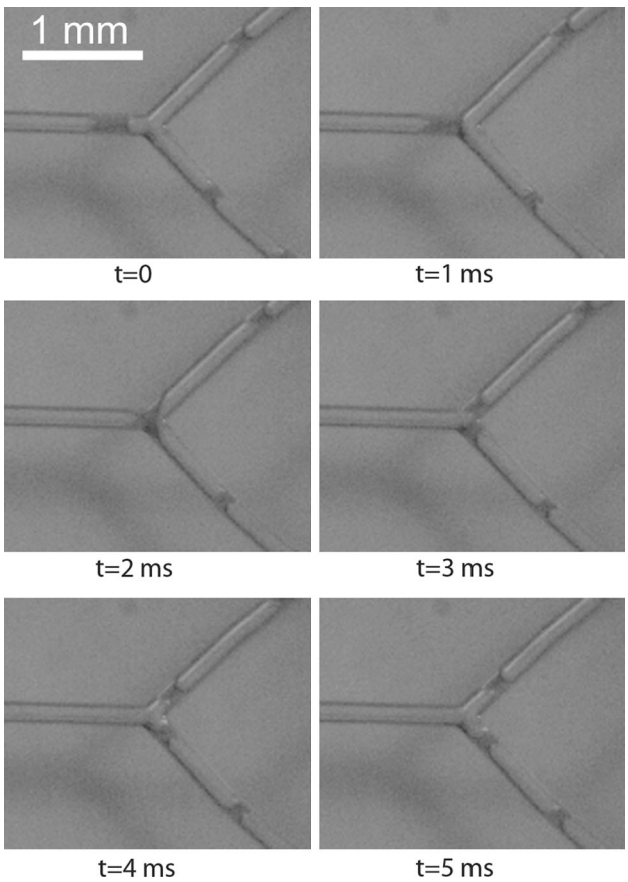

Fig. 5 Splitting exit of a water droplet at bifurcation at 80 μL/min

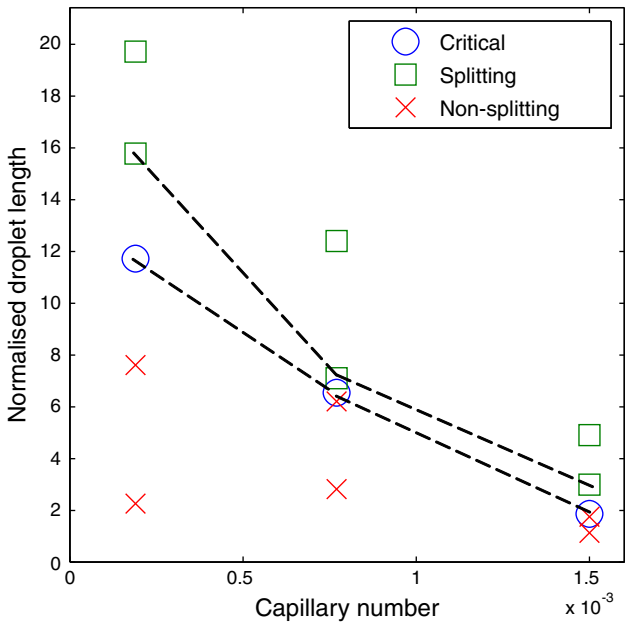

Fig. 6 Droplet behavior at different *Ca*. The droplet lengths are normalized by the channel diameter (180 μm). The critical length is the maximum non-splitting length observed. The *dashed lines* mark the splitting–non-splitting critical region

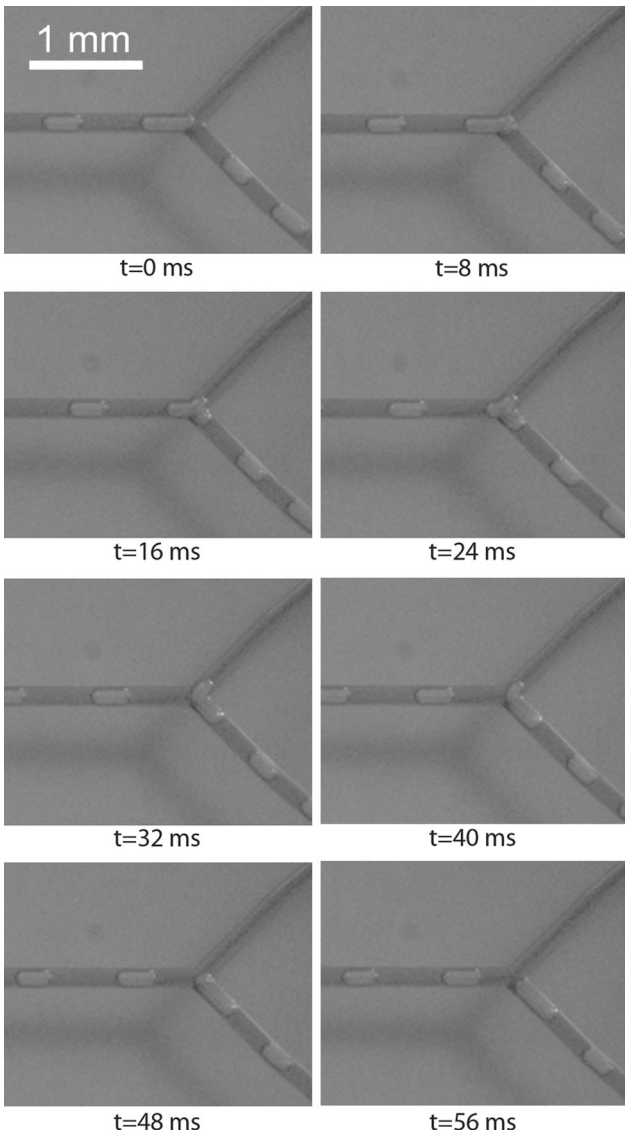

Fig. 7 Non-splitting exit of a CO_2 droplet at bifurcation at 20 μL/min

drawn out in the volume-*Ca* space. A similar map is shown in Fig. 6, where this maximum observed non-splitting droplet length is marked for every flow rate. Additionally, two splitting, and two non-splitting lengths are marked for every flow rate. From the available data, there seems to be a linear dependence of the critical droplet length to the capillary number. However, a logarithmic fit would also describe the behavior fairly well, which would be in correspondence with Carlson et al. (2010). Furthermore, this is the maximum observed non-splitting droplet length, indicating an uncertainty as to what the actual critical length is. For the two highest *Ca*, the uncertainty is small, whereas it is on the order of a few hundred micrometers for the lowest *Ca*.

Figure 7 illustrates a non-splitting behavior, where the droplet extended into both daughter channels after collision with the glass wall (t = 16–40 ms in the figure), but then receded from the top one, with the still intact droplet continuing through the bottom channel. Figure 8 illustrates a splitting behavior. An additional observation from the non-splitting case is that all droplets follow the same trajectory into the same daughter channel.

The initial "selection" of the channel is likely triggered by an uneven flow restriction distribution of the channels. For example, the connecting capillaries could be of slightly different lengths, inducing a slightly lower flow resistance through one of them. After the first $scCO_2$ droplets have entered this channel, this difference becomes more pronounced as the viscosity of $scCO_2$ is lower than the viscosity of water. Thereafter, the majority of the droplets will go through the same channel due to the lower flow resistance.

As the spatial resolution of the camera is rather poor, these measurements are not very precise. They do, however, show a trend. The plotted droplet sizes are single droplets measured. In addition to those plotted, several others in a similar size range were found.

In our experiments, the two bifurcating channels are joined further downstream to form a loop, so that the total pressure loss over both channels is equal. Panizza and coworkers in a series of papers (see, e.g., Engl et al. 2005 and Amon et al. 2013) have investigated the dynamics of smaller non-splitting droplets traveling through more general channel networks. It is interesting to note that with our

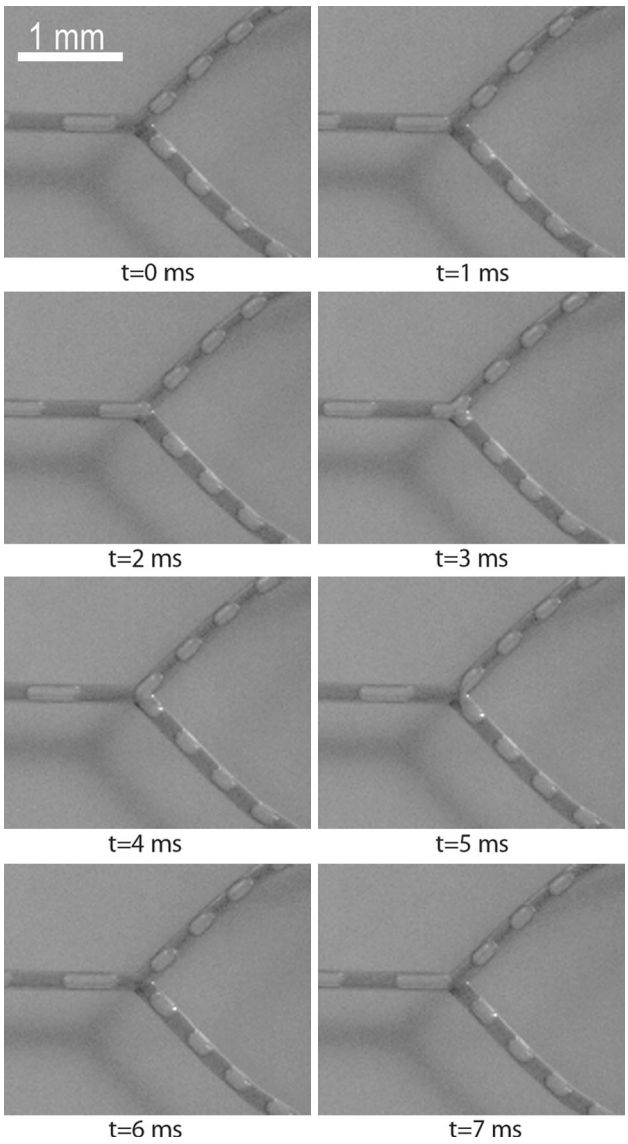

Fig. 8 Splitting exit of a CO_2 droplet at bifurcation at 160 μL/min

elongated low viscosity droplets, the contribution of a droplet is actually to reduce the flow resistance in the channel, as opposed to what is generally the case in the networks studied by Panizza and coworkers.

Supercritical carbon dioxide has today already been much used in stainless steel capillary systems. Just like for ordinary low-pressure microfluidics that does not compete as low-cost disposables, the success of $scCO_2$ microfluidics is coupled to the more advanced geometries possible, providing compact systems with minimal dead volumes, precise interfaces, and different form factors next to each other. We believe that the two main advantages of $scCO_2$ are the potential in processes involving interface chemistry and in processes where concentration by direct gasification gives advantage.

5 Conclusion

The fluid mechanics of supercritical CO_2 and water co-flowing in a double-Y-channel microfluidic glass chip has been studied.

It was found that, due to the low viscosity of $scCO_2$, segmented flow is favored, even at fairly high flow rates. Furthermore, the plug and droplet behavior of water and $scCO_2$ at the bifurcating exit has been characterized, finding that the splitting of $scCO_2$ droplets depends on several parameters, such as wetting characteristics, total flow rate, and droplet length. Water plugs, however, showed no such dependence, instead exhibiting a splitting behavior at all investigated configurations, likely due to the high surface affinity of water and glass.

References

Amon A, Schmit A, Salkin L, Courbin L, Panizza P (2013) Path selection rules for droplet trains in single-lane microfluidic networks. Phys Rev E 88:013012

Assmann N, Kaiser S, von Rohr PR (2012) Supercritical extraction of vanillin in a microfluidic device. J Supercrit Fluids 67:149–154

Barnea D, Luninski Y, Taitel Y (1983) Flow pattern in horizontal and vertical two phase flow in small diameter pipes. Can J Chem Eng 61:617–620

Baroud CN, Gallaire F, Dangla R (2010) Dynamics of microfluidic droplets. Lab Chip 10(16):2032–2045

Blanch-Ojea R, Tiggelaar RM, Pallares J, Grau FX, Gardeniers JGE (2012) Flow of CO_2–ethanol and of CO_2–methanol in a non-adiabatic microfluidic T-junction at high pressures. Microfluid Nanofluidics 12:927–940

Carlson A, Do-Quang M, Amberg G (2010) Droplet dynamics in a bifurcating channel. Int J Multiph Flow 36(5):397–405

Engl W, Roche M, Colin A, Panizza P (2005) Droplet traffic at a simple junction at low capillary numbers. Phys Rev Lett 95: 208304

Georgiadis A, Maitland G, Trusler JPM, Bismarck A (2010) Interfacial tension measurements of the ($H_2O + CO_2$) system at elevated pressures and temperatures. J Chem Eng Data 55(10): 4168–4175

Guillaument R, Erriguible A, Aymonier C, Marre S, Subra-Paternault S (2013) Numerical simulation of dripping to jetting in supercritical fluids/liquid micro coflows. J Supercrit Fluids 81: 15–22

Guillot P, Colin A (2005) Stability of parallel flows in a microchannel after a T junction. Phys Rev E 72:066301

Herrero M, Mendiola JA, Cifuentes A, Ibáñez E (2010) Supercritical fluid extraction: recent advances and applications. J Chromatogr A 1217(16):2495–2511

Lee ML Markides KE (1990) Analytical supercritical fluid chromatography and extraction. Chromatography Conf. Inc., ISBN 0-8425-2394-4

Linstrom PJ, Mallard WG (2014) NIST Chemistry WebBook, NIST Standard Reference Database Number 69, National Institute of Standards and Technology, Gaithersburg MD, 20899. http://webbook.nist.gov. Retrieved 13 Feb 2014

Liu N, Aymonier C, Lecoutre C, Garrabos Y, Marre S (2012) Microfluidic approach for studying CO_2 solubility in water and

brine using confocal Raman spectroscopy. Chem Phys Lett 551:139–143

Marre S, Aymonier C, Subra P, Mignard E (2009) Dripping to jetting transitions observed from supercritical fluid in liquid microcoflows. Appl Phys Lett 95:134105

Marre S, Roig Y, Aymonier C (2012) Supercritical microfluidics: opportunities in flow-through chemistry and materials science. J Supercrit Fluids 66:251–264

Nightingale AM, deMello JC (2013) Segmented flow reactors for nanocrystal synthesis. Adv Mater 25:1813–1821

Ohashi A, Sugaya M, Kim H-B (2011) Development of a microfluidic device for measurement of distribution behaviour between supercritical carbon dioxide and water. Anal Sci 27:567–569

Ribatski G (2013) A critical overview on the recent literature concerning flow boiling and two-phase flows inside micro-scale channels. Exp Heat Transf 26(2–3):198–246

Squires TM, Quake SR (2005) Microfluidics: fluid physics at the nanoliter scale. Rev Mod Phys 77(3):977–1026

Tammisola O, Lundell F, Söderberg LD (2011) Effect of surface tension on global modes of confined wake flows. Phys Fluids 23:014108

Yue J, Luo L, Gonthier Y, Chen G, Yuan Q (2008) An experimental investigation of gas–liquid two-phase flow in single microchannel contactors. Chem Eng Sci 63:4189